Journal of Power Sources 205 (2012) 164–172

Contents lists available at SciVerse ScienceDirect

Journal of Power Sources

journal homepage: www.elsevier.com/locate/jpowsour

Advantageous combination of solid carbon paste and a conducting polymer film as a support of platinum electrocatalyst for methanol fuel cell

Huan Gao, Jian-Bo He*, Yan Wang, Ning Deng

Anhui Key Lab of Controllable Chemical Reaction & Material Chemical Engineering, School of Chemical Engineering, Hefei University of Technology, Hefei 230009, China

ARTICLE INFO

Article history:
Received 22 December 2011
Accepted 5 January 2012
Available online 14 January 2012

Keywords:
Chestnut bur-like particles
Solid carbon paste electrode
Conducting polymer
2-Amino-5-mercapto-1,3,4-thiadiazole
Electrocatalysis
Direct methanol fuel cell

ABSTRACT

Electrodeposition of platinum is comparatively performed on four carbon-based supports: bare glassy carbon electrode (GCE), bare solid carbon paste electrode (sCPE), and a conducting polymer film coated GCE and sCPE. Both the sCPE and poly(2-amino-5-mercapto-1,3,4-thiadiazole) (PAMT) are first used to deposit Pt, with an aim of improving electrocatalytic activity of Pt toward methanol oxidation. Scanning electron microscopy shows that chestnut bur-like Pt particles with numerous nanothorns are deposited on all the supports by controlling deposition potential and time, and the particles on the PAMT film supported on the both substrates are found in two size fractions (<1 μm and 2–3 μm). Voltammetric data indicate that both the sCPE and the PAMT contribute to increase electrochemical active area of Pt catalyst and therefore have a positive effect on Pt's electrocatalytic activity, in comparison with the GCE and the uncoated supports, respectively. Moreover, impedance spectroscopy reveals that the sCPE-supported PAMT facilitates the electron transfer kinetics of methanol oxidation, whereas the GCE-supported PAMT gives an opposite effect on the electron transfer. This work shows that the solid carbon paste is superior to glassy carbon for use in combination with a conducting polymer as a support of Pt electrocatalyst.

1. Introduction

Direct methanol fuel cell (DMFC) is considered a promising power source for electric vehicles and electronic portable devices due to its simple design, low operating temperature, and convenient fuel storage and supply [1,2]. One of the major interest in current research on DMFCs is how to minimize the loadings of noble metals (mainly platinum or Pt-based alloys), meanwhile to improve the relatively slow kinetics of methanol oxidation reaction. As a general strategy for this problem, such metal catalysts are highly dispersed on conductive supports [2,3]. The characteristics of the catalyst supports, i.e., chemical composition, surface functional group, specific surface area, porosity, morphology, electronic conductivity and corrosion resistance, have strong effects on the properties and performance of the supported catalysts, such as metal particle size, size distribution, morphology, dispersion and stability [1,3,4].

Carbon materials, such as glassy carbon [3,5], carbon black [6], carbon nanotube (CNT) [4,6], graphene [7], carbon nanofiber [8,9], carbon nanocoil [10] and mesoporous carbon [11], are the most common catalyst supports because of their good electric conductivity, relative stability in various media and high specific surface area. In recent years, hybrid carbon-based materials, including carbon-polymer [2,12,13], carbon-polymer-oxide [14], carbon–ceramic [15], carbon–ceramic-polymer [16], etc. have been extensively studied as fuel cell catalyst supports. These hybrid materials, possessing the properties of each component, or even with a synergistic effect, would present improved characteristics and electrocatalytic activity with respect to the individual components [17].

Conducting polymers (CPs) deposited on carbon substrates are very favorable and attractive hybrid supports for catalyst particles, and some promising results were recently reported for Pt-based nanocatalysts dispersed on CPs, such as polyaniline (PANI) [2,3] and PANI-containing composites [13,18], polyindole (PIn) [12,19], poly (*o*-phenylenediamine) (PoPD) [16,20], poly (3,4-ethylenedioxythiophene) (PEDOT) [14,21,22], polytyramine (PTy) [23], poly(3-methylthiophene) (P3MT) [24,25], poly (*o*-aminophenols) (PoAP) [26], poly(N-acetylaniline) [27] and poly (*m*-toluidine) (PMT) [28]. CPs offer great advantages of high accessible surface area, low resistance, good stability [29] and desirable film thickness, and allow straightforward electrochemical preparation on the substrates. CPs function as redox mediators not only by electron but also proton transfer [29] between the electrodes and the electroactive reactants, compensating for the shortcoming of plain carbon materials that do not contribute to proton transport involved in fuel electrooxidation reactions [20]. In additon, CP matrixes with high surface area are suitable for highly

* Corresponding author. Tel.: +86 551 2901288; fax: +86 551 2901450.
E-mail address: jbhe@hfut.edu.cn (J.-B. He).

0378-7753/$ – see front matter © 2012 Elsevier B.V. All rights reserved.
doi:10.1016/j.jpowsour.2012.01.062

dispersed deposition of Pt particles [13,23]. Such Pt particles with very small sizes are less able to form multiple metal–carbon bonds than bulk Pt, therefore display higher resistance to self-poisoning by CO formed during methanol oxidation [28–30].

Recent years, various liquid oil-bound carbon pastes are also used as the substrates of CP films for catalytic oxidation of methanol, prepared from graphite powders and paraffin [19,31–34], multi-walled carbon nanotubes (MWCNTs) and paraffin [35], graphite powders and MWCNTs and paraffin [28,36], graphite powders and silicon oil [37], etc. The carbon paste electrodes offer great advantages of low noise and background currents in a wide range of potentials, and allow simple renewal and easy modification on their surfaces [38,39].

In the present work, four carbon-based supports are selected for electrodeposition of Pt particles, with a hope to affect the particle size, size distribution and morphology, and then improve the electrocatalytic activity of Pt particles toward methanol oxidation in acidic media. The supports include bare glassy carbon electrode (GCE), bare solid carbon paste electrode (sCPE), and a CP film coated GCE and sCPE. The CP film is composed of poly(2-amino-5-mercapto-1,3,4-thiadiazole) (PAMT) that is electrodeposited onto the GCE and sCPE surfaces. Both the sCPE substrate and the PAMT film are used for the first time to deposit Pt. Solid paraffin wax as an uncommon binder of carbon powders results in 'solid-like' or 'pseudo' carbon pastes that have significant advantages over the common liquid oil-bound ones, such as robust in operation, improved reproducibility, low residual currents, and better stability against organic solvents [39,40]. As for the PAMT film, its excellent charge transfer properties have been evidenced in a recent work of our group, in which a PAMT modified electrode was fabricated for the purpose of electroanalysis [41].

2. Experimental

2.1. Chemicals and solutions

Spectrograde graphite powders (320 mesh) and spectrograde paraffin wax (solidification point 56–58 °C) were purchased from China-Reagent group for preparing the solid carbon paste electrode. 2-Amino-5-mercapto-1,3,4-thiadiazole (AMT, ≥98%) was purchased from Alfa Aesar. $H_2PtCl_6{\cdot}6H_2O$ (≥37.0% Pt) and sulfuric acid (AR) were from Chemical Regent Company of Shanghai, and were used as received. All other chemicals were of analytical grade from China-Reagent group. High pure N_2 was used to deaerate the solutions. Doubly-distilled water from an all-glass distillatory apparatus was used as solvent.

The monomer solution for electropolymerization was 0.5 mmol dm^{-3} AMT in 0.1 mol dm^{-3} H_2SO_4. The solution for electrodeposition of platinum particles contained 5.0 mmol dm^{-3} H_2PtCl_6 and 0.5 mol dm^{-3} H_2SO_4. The supporting electrolytes for methanol oxidation were 0.5 mol dm^{-3} H_2SO_4 plus CH_3OH with different concentrations.

2.2. Electrode preparation

The solid carbon paste was made from dry graphite powders and paraffin wax (5:2, w/w). The electrode body was a polystyrene hollow tube with inner diameter of 3.0 mm. The tube was tightly impacted with a copper rod, leaving a cavity of 2 mm depth at one end. The solid wax was heated until molten, and then mixed with the graphite powders in a watch glass with a glass rod until a well blended paste was obtained. The paste was firmly pressed into the cavity of the electrode body forming a bare sCPE with a geometric area of 0.0707 cm^2. This area was used for calculation of current density (j). A commercial available glassy carbon disk electrode with the same diameter as the sCPE was used for comparison.

The bare sCPE and GCE were polished successively with 1000 and 4000 grit emery papers followed by ultrasonically cleaning: the former was rinsed in double distilled water for 5 s, the latter was in 1:1 (v/v) ethanol, 1:1 (v/v) nitric acid and distilled water each for 2 min, respectively. Prior to use, the cleaned substrates were subjected to repetitive potential cycling between −0.4 and 1.6 V at 0.5 V s^{-1} in 1.0 mol dm^{-3} KCl until the background current was obtained.

The cleaned substrates were modified by cyclic potential scan between −0.2 and 1.7 V (vs. SCE) at 50 mV s^{-1} in the AMT monomer solution. The cycle number for the electropolymerization was optimized in the range of 0–100 cycles according to the electrocatalytic activity toward methanol oxidation. In this way, PAMT film was electrodeposited on the substrate surface forming PAMT-modified carbon paste electrode (PAMT/sCPE) or PAMT-modified glass carbon electrode (PAMT/GCE). The prepared electrode was rinsed with distilled water and cleaned by potential cycling in 1.0 mol dm^{-3} KCl to remove adsorbed substances.

Platinum particles were electrodeposited onto both the sCPE and GCE substrates with or without the PAMT coatings, at a constant potential of −0.2 V (vs. SCE) in the H_2PtCl_6-containing solution. Current was monitored for the intended duration of electrodeposition, and the charge was calculated for estimating the level of Pt loading. The final Pt-loaded electrodes are denoted as Pt/sCPE, Pt/GCE, Pt/PAMT/sCPE and Pt/PAMT/GCE.

After Pt particles incorporation, the electrodes were rinsed with distilled water and cleaned in 0.5 mol dm^{-3} H_2SO_4 by potential cycling between −0.3 V and 1.3 V at υ = 50 mV s^{-1} until a reproducible cyclic voltammogram was obtained.

2.3. Apparatus and procedures

Cyclic voltammetry (CV), electrochemical impedance spectroscopy (EIS) and chronoamperometry were performed on the CHI 660C electrochemical workstation (CH Instruments Co., Shanghai, China). A three-electrode system was used, which was composed of a saturated calomel reference electrode (SCE), a platinum coil counter electrode, and a working electrode. The Pt-loaded working electrodes included Pt/sCPE, Pt/PAMT/sCPE, Pt/GCE and Pt/PAMT/GCE for comparison. The electrolyte solutions were deaerated with high pure N_2 for about 15 min prior to experimentation. All experiments were carried out at room temperatures (approximately 25 °C).

Field-emission scanning electron microscope (FESEM) images of the four Pt-loaded electrodes were collected using a FEI Sirion 200 field-emission scanning electron microscope coupled with Oxford EDAX energy dispersion spectrum (EDS) analyzer.

3. Results and discussion

3.1. Electrodeposition of PAMT and Pt

Electrooxidative polymerization of AMT monomer on GCE or sCPE was carried out by multi-cycle potential scan in an acidic aqueous electrolyte, to form a polymer coating on the substrates according to the reaction [41]:

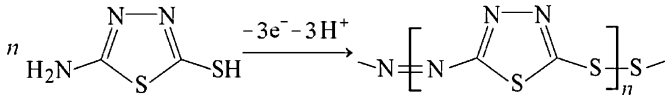

The CVs for the polymerization of AMT on GCE and sCPE are shown in Fig. 1, in which the voltammetric parameters were selected on the basis of reference [41]. The cycle number for the polymerization was set in a range of 5–75 cycles to study the effect

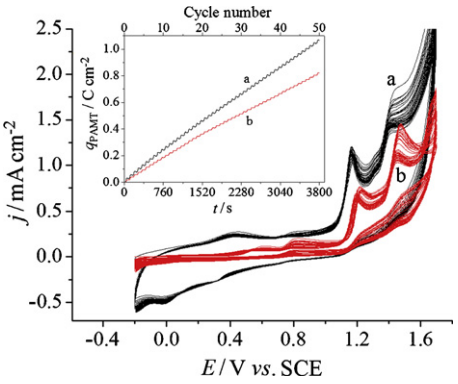

Fig. 1. CVs for electropolymerization of AMT on GCE (a) and sCPE (b) in 0.5 mmol dm^{-3} AMT + 0.5 mol dm^{-3} H_2SO_4. GCE and sCPE area: 0.0707 cm^2, scan rate: 50 mV s^{-1}, cycle number: 50 cycles. Inset: voltammetric charge as a function of cycle number.

of PAMT loading level on methanol oxidation. For this purpose, the amount of coulombic charge consumed for the polymerization was estimated by integrating the multi-cycle voltammetric current with time. The resulting area-specific charges (q_{PAMT}) present nearly linear increase with cycle number (inset of Fig. 1), yielding two slopes of 21.2 and 16.4 mC cm^{-2} per cycle for the substrates GCE and sCPE, respectively. The value of q_{PAMT} was used to calculate the area-specific mass (m_{PAMT}) of PAMT according to Faraday law, $m_{PAMT} = q_{PAMT}M_{AMT}/nF$, where n the electron transfer number per molecule of AMT ($n = 3$), M_{AMT} the molar mass of AMT (133.2 g mol^{-1}), and F the Faraday constant (96484.6 C mol^{-1}). From the two slopes above, the area-specific masses of the PAMT deposited on GCE and sCPE per cycle were estimated to be 9.7 and 7.5 μg cm^{-2}, respectively.

For deposition of Pt particles, both potentiostatic and multi-cycle potentiodynamic methods were comparatively attempted in a solution containing 0.5 mmol dm^{-3} H_2PtCl_6 and 0.5 mol dm^{-3} H_2SO_4, and the former with a constant potential of −0.2 V (vs. SCE) was selected in the following experiments. The time for Pt deposition was set from 5 to 75 min to study the effect of Pt loading level on methanol oxidation. The area-specific charges (q_{Pt}) consumed during Pt deposition were obtained by integrating the experimental chronoamperometric curves. There is a difficulty, however, in determining the exact charges consumed for Pt deposition, due to the side reactions such as proton reduction occurring on the already deposited Pt. As an approximation, a current efficiency of 52% reported in Ref. [42] was taken for estimating the area-specific mass (m_{Pt}) of Pt loading: $m_{Pt} = (q_{Pt}M_{Pt}/nF) \times 0.52$ ($n = 4$, $M_{Pt} = 195.1$ g mol^{-1}). For example, 20 min of deposition at −0.2 V produced 0.30 and 0.27 mg cm^{-2} Pt on the sCPE and PAMT/sCPE, respectively.

3.2. Morphology of Pt deposits

The surface morphologies of the four Pt-loaded electrodes were characterized with FESEM. Fig. 2 shows the micrographs of Pt/GCE, Pt/PAMT/GCE, Pt/sCPE and Pt/PAMT/sCPE prepared under identical conditions. Nano/microspheres, typically in diameters from 0.1 to 1 μm, were formed on all the four supports, and their chemical composition was confirmed as platinum by EDX analysis (data not shown). Moreover, agglomerated Pt particles with diameters mostly from 2 to 3 μm were observed on the two PAMT-coated substrates (Fig. 2B and D). These agglomerates are generally considered to be formed by successive nucleation: primary nucleation of a Pt deposit followed by secondary nucleation on the predeposited Pt surface [22]. This suggests that the PAMT film-supported Pt particles possess high activity of surface defects allowing the secondary nucleation. The aggregated structure was therefore formed, accompanied by a decrease in degree of surface coverage by Pt particles, as observed from comparison of Fig. 2A and C with B and D. A previous study focusing on the influence of particle agglomeration [43] indicated that the Pt agglomerates, due to high concentration of surface defects, may show remarkably enhanced catalytic activity in comparison to either isolated Pt nanopraticles or polycrystalline Pt foil.

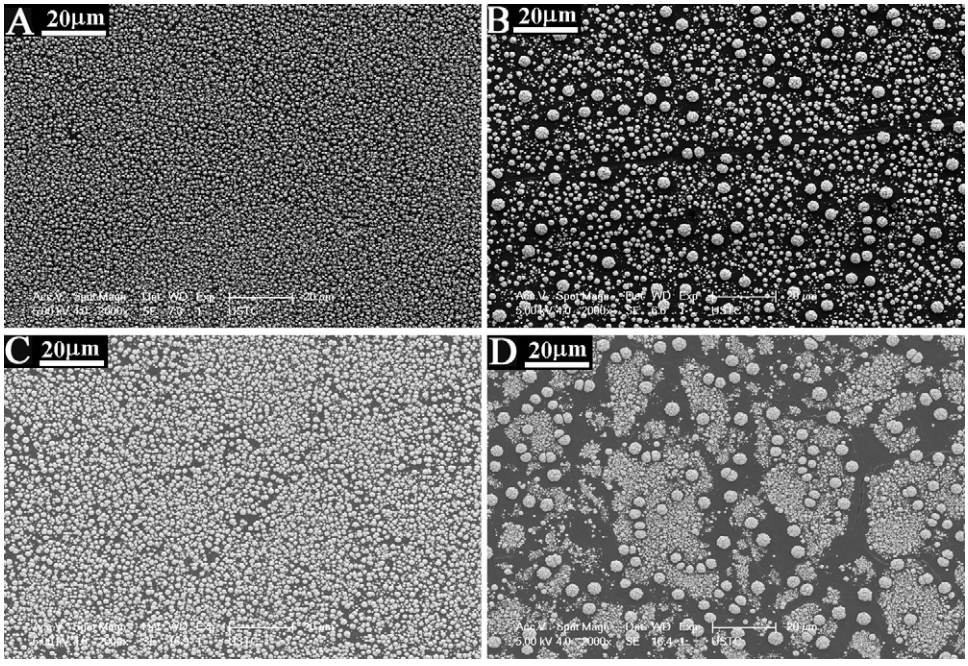

Fig. 2. FESEM images of Pt/GCE (A), Pt/PAMT/GCE (B), Pt/sCPE (C) and Pt/PAMT/sCPE (D). The PAMT on the substrates was deposited from 0.5 mmol dm^{-3} AMT + 0.5 mol dm^{-3} H_2SO_4 by CV scan between −0.2 V and 1.7 V (vs. SCE) at 50 mV s^{-1} for 50 cycles. The Pt particles were deposited from 5.0 mmol dm^{-3} H_2PtCl_6 + 0.5 mol dm^{-3} H_2SO_4 at a constant potential of −0.20 V (vs. SCE) for 20 min.

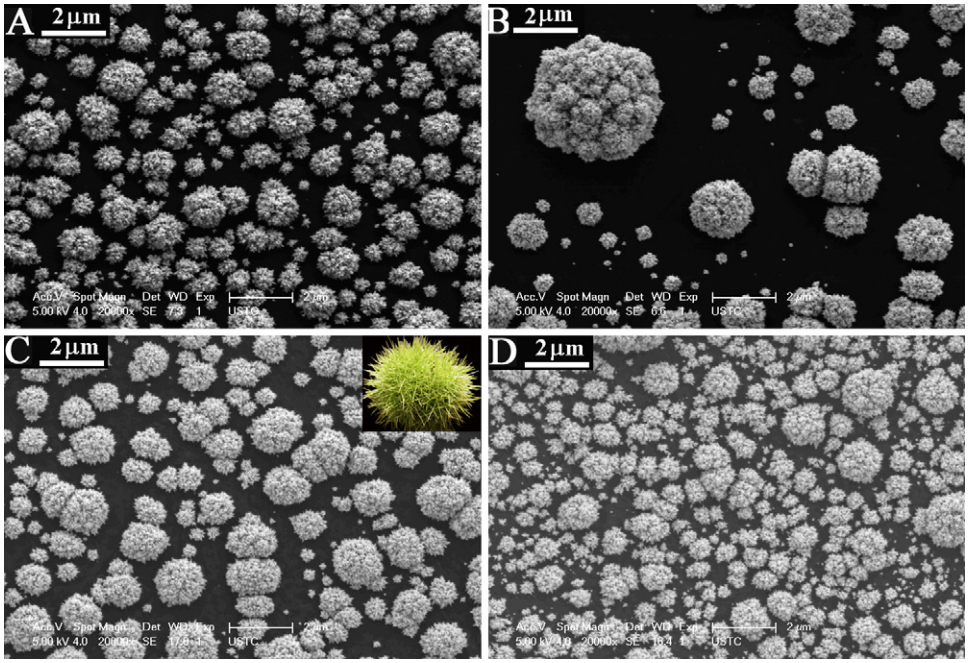

Fig. 3. FESEM images of Pt/GCE (A), Pt/PAMT/GCE (B), Pt/sCPE (C) and Pt/PAMT/sCPE (D) in a higher magnification than in Fig. 2. The inset shows a picture of a chestnut bur.

There is not discernible difference in shape, size, size distribution and surface uniformity between the Pt particles deposited on the bare GCE and on the bare sCPE (compare the Fig. 2A and C), although there were great differences in substrate composition (containing wax or not) and carbon structure between the two bare substrates. In the presence of the PAMT film, however, the size of the isolated Pt praticles was reduced considerably only on the PAMT/sCPE (mostly 0.1–0.5 μm, Fig. 2D), contributing to the increase in specific surface area of the particles.

Fig. 3 shows the micrographs of the four electrodes at a higher magnification. It can be seen that the Pt particles on all the four supports show an impressive chestnut bur-like morphology with numerous nanoscale thorns. The nanothorns have sharp needle-points and are arranged on the surface in the radial direction. This chestnut bur-like structure, rarely or never reported for Pt particles, is expected to be favorable for improving the catalytic activity due to the highly developed specific surface with various active sites. A similar hedgehog-shaped morphology, with many nanoscale leaf-like flakes on the surface, was recently prepared for gold particles from electrodeposition, resulting in enhanced voltammetric responses [44].

3.3. Electrochemical active surface area of Pt deposits

The electrochemical active surface areas of Pt deposits on the four supports were determined by the voltammetric measurements in 0.5 mol dm^{-3} H_2SO_4. Fig. 4 shows the typical multiple peaks in the lower potential range of −0.2 to 0.1 V, which are related to hydrogen reductive adsorption/oxidative desorption on a Pt surface [16]. The anodic peak at the higher potentials around 0.8 V and its cathodic counterpart at about 0.55 V are due to the formation and reduction of the Pt oxide monolayer [6].

The coulombic charge for hydrogen oxidative desorption from the Pt surface was determined by integrating the anodic current between −0.2 and 0.1 V after subtraction of the double layer current. The obtained charges can be used to characterize the electrochemical active surface area (A_{EAS}) of Pt deposits [6], assuming a specific charge of 210 μC cm^{-2} [45] for hydrogen desorption from an atomically smooth Pt surface. The A_{EAS} values were calculated to be 19, 28, 36, and 60.5 (cm^2 Pt)/(cm^2 geometric area of electrode), respectively, for the Pt/GCE, Pt/PAMT/GCE, Pt/sCPE and Pt/PAMT/sCPE used in Fig. 4. The active specific surface areas of Pt particles on the four electrodes were then estimated to be 105, 155, 120 and 224 cm^2 mg^{-1} sequentially, considering the specific masses of Pt deposits as in Section 3.1. The highest specific surface was obtained at Pt/PAMT/sCPE (approximately with 0.375 mg PAMT cm^{-2} and 0.27 mg Pt cm^{-2}), suggesting that the sCPE-supported PAMT film is the most promising candidate as a Pt support among the four electrodes. In addition, the bare sCPE is a better direct support for Pt than the bare GCE, although with smaller real area than the latter due to the presence of wax.

3.4. Catalytic oxidation of methanol by Pt deposits

Methanol oxidation at the Pt surface showed the characteristic double voltammetric peaks (P_F and P_R, Fig. 5A) that appeared in the forward and reverse scans, respectively. The peak P_F at around 0.65 V is assigned to the oxidation of methanol in multiple steps, producing carboxyl intermediates together with strongly adsorbed CO species [25,28,46]. With the scan positive-going, the peak P_F

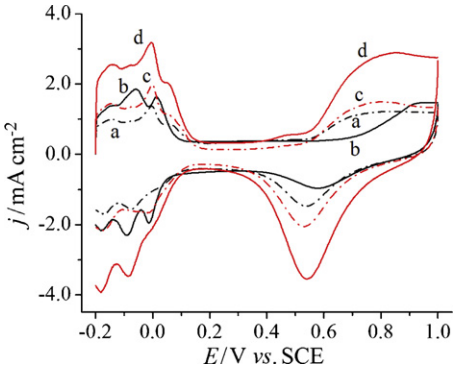

Fig. 4. CVs of Pt/GCE (a), Pt/PAMT/GCE (b), Pt/sCPE (c) and Pt/PAMT/sCPE (d) in 0.5 mol dm^{-3} H_2SO_4. GCE and sCPE area: 0.0707 cm^2, scan rate: 50 mV s^{-1}. The four electrodes were prepared under the same conditions as in Fig. 2.

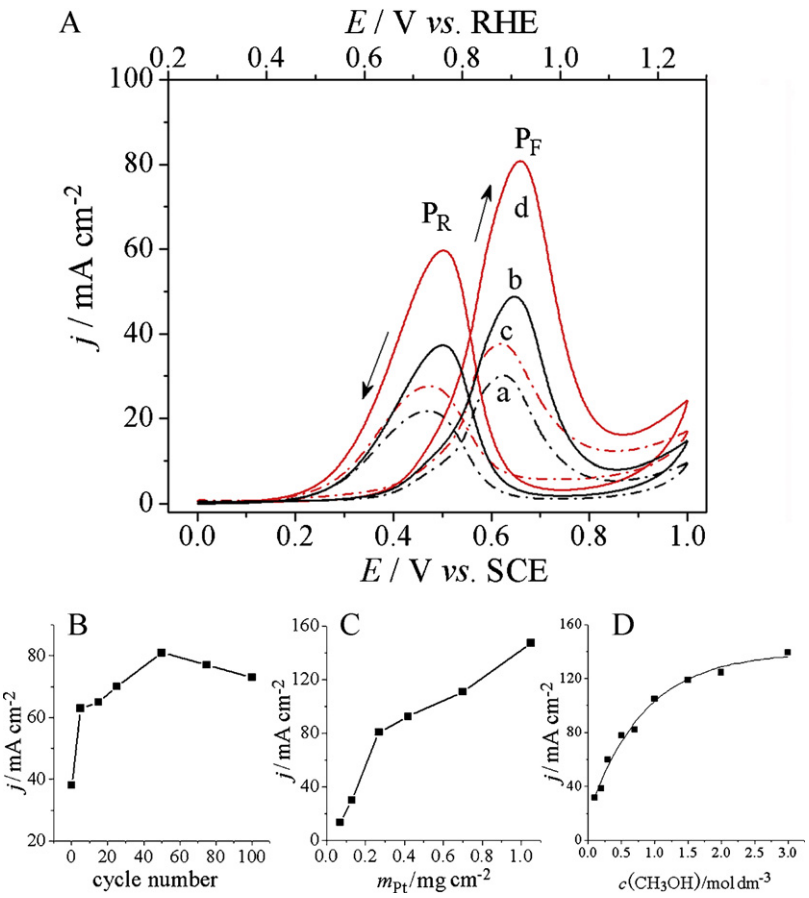

Fig. 5. CVs of Pt/GCE (a), Pt/PAMT/GCE (b), Pt/sCPE (c) and Pt/PAMT/sCPE (d) in 0.5 mol dm^{-3} H_2SO_4 + 0.5 mol dm^{-3} CH_3OH. GCE and sCPE area: 0.0707 cm^2, scan rate: 50 mV s^{-1}. The four anodes were prepared under the same conditions as in Fig. 2. The lower three panels show the P_F peak current density at Pt/PAMT/sCPEs as a function of cycle number for PAMT deposition (B), Pt loading (C) and CH_3OH concentration (D). The Pt/PAMT/sCPEs were prepared under the same conditions except where indicated.

was followed by a current drop due to the formation of Pt oxide (PtO) that passivated the surface, and subsequently by a current rise arising from the potential-driven oxidation on the surface of Pt oxide [25]. The Pt/PAMT/sCPE showed the highest P_F peak current density (j_p) of 80 mA cm^{-2} that is about two times as high as that of the Pt/sCPE (38 mA cm^{-2}). Similarly, the Pt/PAMT/GCE yielded a significantly higher peak current density (50 mA cm^{-2}) than did the Pt/GCE (30 mA cm^{-2}). Therefore, the PAMT film on both the substrates played an important role in promoting methanol oxidation at Pt particles. In addition, the substrate sCPE contributed more than the GCE to the catalytic activity of Pt, whether with or without PAMT film on them. The enhancement of the catalytic activity can be attributed to the increase in electrochemical active surface area (described in Section 3.3) of Pt deposits as well as the occurrence of the Pt agglomerates on the PAMT film (Fig. 2B and D).

The reverse anodic peak P_R at around 0.5 V is attributed to the oxidative removal of CO and other residual carbon species formed on the electrodes in the forward scan [7]. Their oxidation reactions unusually occurred at relatively negative potentials, following the electroreduction of Pt oxide (as indicated by the first cathodic peak in Fig. 4) that produced a rather reduced/non-poisoned Pt surface [25].

Fig. 5B shows the P_F peak current as a function of the PAMT amount deposited on the sCPE. The peak current of methanol oxidation at Pt/PAMT/sCPE increased significantly with increasing circle number for the PAMT deposition from the monomer solution, until the cycle number was up to about 50 cycles. Fig. 5C shows the P_F peak current as a function of the area-specific mass of Pt deposits on the PAMT/sCPE. The mass of Pt was determined from deposition time as described in Section 3.1. The peak current of methanol oxidation increased continuously with the Pt deposition time in the test time scale up to 75 min, at first sharply (<20 min) and then more gradually. The peak currents per unit of Pt mass were then calculated to be 193, 231, 300, 220, 159 and 140 mA (mg Pt)$^{-1}$ for the deposition time of 5, 10, 20, 30, 50 and 75 min, respectively, indicating that 20 min of deposition time resulted in the highest mass-specific activity of Pt deposits toward methanol oxidation. Fig. 5D shows the P_F peak current as a function of methanol concentration. The peak current increased with increasing methanol concentration up to 3.0 mol dm^{-3}, sharply below 1.0 mol dm^{-3} and then more gradually.

Tables 1 and 2 list some composite electrodes recently reported for use in catalytic oxidation of methanol. Among these electrodes the Pt/PoPD/CCE [16] generated the highest methanol peak current density, with a porous carbon–ceramic electrode (CCE) as the support that provided a large surface area for the Pt deposition (Pt loading, 0.6 mg cm^{-2}). As shown in Tables 1 and 2, the Pt/PAMT/sCPE prepared in the present work exhibited excellent electrocatalytic activity toward methanol oxidation.

3.5. EIS characterization

The charge-transfer properties of the electrode interfaces at a series of potentials were analyzed using EIS. Fig. 6 shows the highly potential-dependent Nyquist plots of the four anodes in 0.5 mol dm^{-3} CH_3OH + 0.5 mol dm^{-3} H_2SO_4. The applied bias

Table 1
Recently reported polymer-supported Pt electrodes for electrocatalytic oxidation of methanol in acidic media. All the values of j_p are referred to the electrode geometric areas available in the respective literature. All the peak potentials quoted in this table were converted to values vs. RHE (reversible hydrogen electrode) in the same solutions for comparison.

Composite electrodes	CV scan for CH_3OH oxidation				Refs.
	c (mol dm^{-3})	v (mV s^{-1})	j_p (mA cm^{-2})	E_p (V) vs. RHE	
PANI/Pt/GC	CH_3OH: 3.0 H_2SO_4: 0.5	50	14	0.90	[2]
Pt/PMI/GC	CH_3OH: 1.0 H_2SO_4: 0.5	50	68	0.92	[12]
Pt/PANI-PAMA/ITO	CH_3OH: 0.1 H_2SO_4: 0.5	10	1.6	0.97	[13]
Pt/PEDOT-V_2O_5/GC	CH_3OH: 1.0 H_2SO_4: 1.0	50	57	1.22	[14]
Pt/PoPD/CCE	CH_3OH: 0.5 H_2SO_4: 0.3	50	117	1.08	[16]
Pt/$PoPD_{nanotube}$/Naf/Gr	CH_3OH: 1.0 H_2SO_4: 0.5	50	84	0.98	[20]
Pt/PEDOT/C	CH_3OH: 1.0 H_2SO_4: 0.1	5	5.7	0.91	[21]
Pt/PEDOT/C	CH_3OH: 1.0 H_2SO_4: 0.1	5	8.8	0.90	[22]
Pt/PTy/GC	CH_3OH: 3.7 H_2SO_4: 0.5	50	8.8	0.93	[23]
Pt/P3MT/GC	CH_3OH: 0.1 $HClO_4$: 0.1	50	4.5	0.92	[24]
Pt/PANI/Nc	CH_3OH: 0.5 H_2SO_4: 0.5	50	8.5	0.96	[47]
Pt/PAMT/sCPE	CH_3OH: 0.5 H_2SO_4: 0.5	50	80	0.92	This work
	CH_3OH: 1.0 H_2SO_4: 0.5	50	104	0.93	

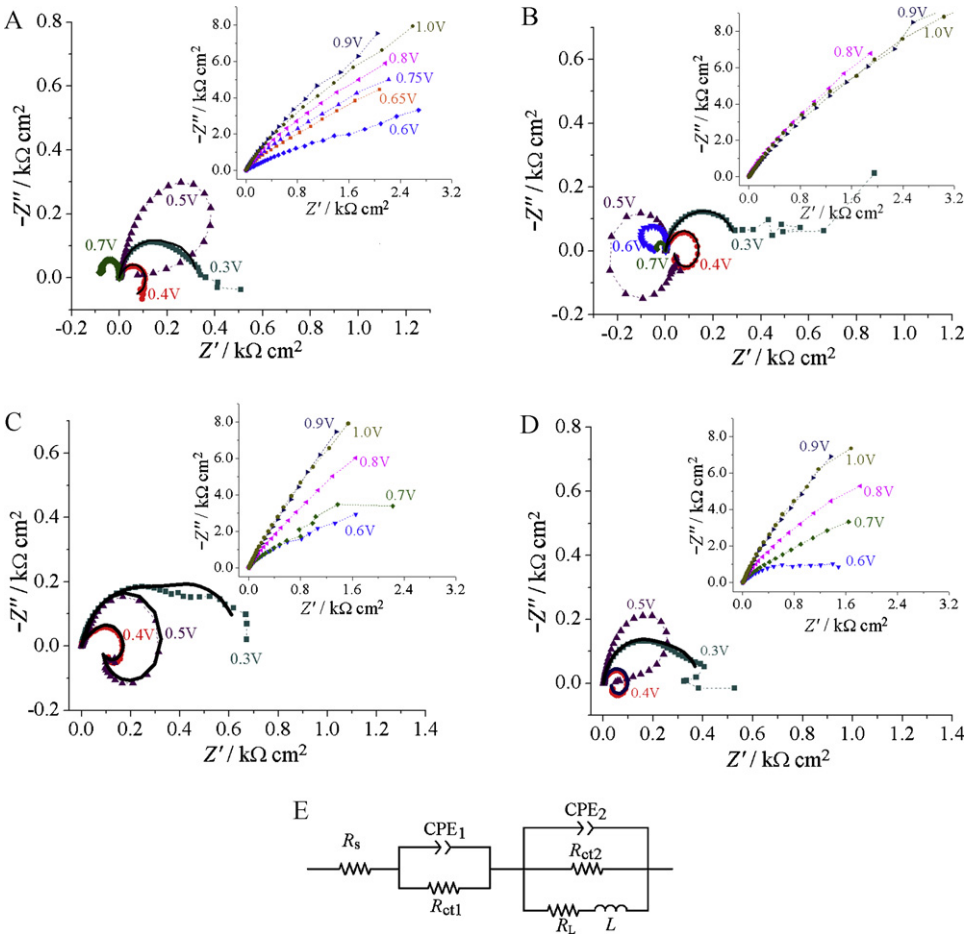

Fig. 6. Nyquist plots of Pt/GCE (A), Pt/PAMT/GCE (B), Pt/sCPE (C) and Pt/PAMT/sCPE (D) in 0.5 mol dm^{-3} CH_3OH + 0.5 mol dm^{-3} H_2SO_4. The electrodes were prepared under the same conditions as in Fig. 2. Frequency range: 100 kHz–0.01 Hz; amplitude: 10 mV; bias potential: 0.3–1.0 V vs. SCE as indicated beside each spectrum. The solid curves are the simulated plots using the equivalent circuit shown in the panel (E).

Table 2
Previously reported carbon paste based electrodes for electrocatalytic oxidation of methanol. All the values of j_p are referred to the electrode geometric areas available in the respective literature. All the peak potentials quoted in this table were converted to values vs. RHE in the same solutions for comparison.

Materials for carbon pastes	Modifiers	CV scan for CH_3OH oxidation				Refs.
		c (mol dm^{-3})	ν (mV s^{-1})	j_p (mA cm^{-2})	E_p (V) vs. RHE	
Graphite powder + paraffin	Pt-Ni/PIn	CH_3OH: 0.5 $HClO_4$: 1.0	25	45	0.88	[19]
Graphite powder + MWCNT + paraffin	Pt/PMT/TX-100	CH_3OH: 1.4 H_2SO_4: 0.5	50	24.8	0.88	[28]
Graphite particles + NiY + paraffin oil	Ni-NiY	CH_3OH: 0.5 NaOH: 0.1	20	13.2	1.79	[31]
Graphite powder + paraffin	Ni/PDAN	CH_3OH: 0.57 NaOH: 0.1	10	1.43	1.63	[32]
Graphite powder + paraffin	Ni/CTAB-PMT	CH_3OH: 0.19 NaOH: 0.1	20	40	1.79	[33]
Graphite powder + paraffin	Ni/PANI	CH_3OH: 0.5 NaOH: 0.1	25	16.7	1.56	[34]
MWCNT + paraffin oil	Ni(II)-Qu	CH_3OH: 0.4 NaOH: 0.1	20	18.5	1.71	[35]
Graphite powder + MWCNT + paraffin	Ni/PoT/TX-100	CH_3OH: 0.24 NaOH: 0.1	20	18.7	1.66	[36]
Graphite powder + silicon oil	Ni/PoAP	CH_3OH: 0.45 NaOH: 0.1	50	1.65	1.58	[37]
Carbon paste	Ni/SDS-PoAP	CH_3OH: 0.76 NaOH: 0.1	20	17.1	1.72	[48]
Graphite powder + solid wax	Pt/PAMT	CH_3OH: 0.5 H_2SO_4: 0.5	50	80	0.92	This work

potentials started from 0.3 V vs. SCE, i.e., the onset potential of the voltammetric peak P_F (see Fig. 5A). At the lower potentials of 0.3, 0.4 and 0.5 V vs. SCE, all the spectra exhibit an irregular circle or arc of circle, which decreased in size with the potential changing from 0.3 to 0.4 V. The smallest impedance arc was obtained at 0.4 V for all the anodes, indicating a smallest charge-transfer resistance (R_{ct}) due to the efficient removal of the intermediate CO_{ads} allowed at this potential. What is more, all the spectra at 0.4 V present a low frequency loop extending to the fourth quadrant, reflecting a typical pseudo-inductive behavior. The same feature was also observed at 0.5 V but only for the Pt/sCPE (Fig. 6C). This inductive behavior has been explained by Müller et al. [49] using the kinetic theory derived by Harrington and Conway [50] for the reactions involving intermediate adsorbates. Oxidative removal of CO_{ads} lead to the regeneration of active sites; the resulting relaxation phenomena yields an increase in potential followed by an increase in current with a phase delay, such that the potential-dependent change in capacitance resembles an inductance [49,51–53].

The pseudo-inductive impedances were fitted using the equivalent circuit [53] shown in Fig. 6E, where R_s is the solution resistance, CPE_1 and R_{ct1} are the high frequency constant phase element and high frequency resistance corresponding to the charge-transfer process at the outermost surface of the catalysts, CPE_2 and R_{ct2} are the constant phase element and charge-transfer resistance within the porous Pt particles, R_L and L are the low frequency resistance and low frequency inductance due to the adsorbed CO layer, respectively. The constant phase elements are used instead of capacitors to account for the inhomogeneity of the film. The fitting (solid) curves were overlaid in Fig. 6 showing good agreement with the measured data points.

The fitting parameters are listed in Table 3. The values of R_{ct1} at Pt/PAMT/GCE under the potentials of 0.3 and 0.4 V were about 1.5 and 5 times as large as those at Pt/GCE, respectively, reflecting a negative effect of GCE-supported PAMT film on electron transfer kinetics of methanol oxidation. On the contrary, both the values of R_{ct1} and R_{ct2} at Pt/PAMT/sCPE were smaller than their respective values at Pt/sCPE under every identical potential, showing a facilitating effect of sCPE-supported PAMT film on electron transfer. Similar opposite effects were previously reported based on the EIS data of a PAMT/GCE [54] and of a PAMT/sCPE [41] in ferri/ferrocyanide solutions, by John's and our groups, respectively. That is, the charge transfer resistance (R_{ct}) of the ferri/ferrocyanide redox couple increased with increasing PAMT amount deposited on the GCE [54], but the opposite change in R_{ct} was obtained when the sCPE was used as the substrate [41].

The four insets in Fig. 6 show the Nyquist plots recorded in the higher potential range, that is, 0.6–0.65 V and 0.75–1.0 V for Pt/GCE, 0.8–1.0 V for Pt/PAMT/GCE, 0.6–1.0 V for Pt/sCPE and Pt/PAMT/sCPE, respectively. All the impedances arcs there increased in size with increasing potential up to 0.9 V, due to the increasing Pt oxides formed on the Pt surface hindering the oxidation of methanol and CO_{ads}. The impedances arcs showed no change or a little decrease in size as the potential was further shifted from 0.9 to 1.0 V driving the oxidation of CO_{ads} to CO_2 on the surface of Pt oxides (see Fig. 5A). The same opposite effects of the PAMT film as described above were also observed in the higher potential range, by comparing the relative sizes of the impedances arcs among these anodes. The GCE-supported PAMT film led to an increase in arc size and therefore in electron transfer resistance (compare the insets of Fig. 6A and B), whereas the sCPE-supported PAMT film had an opposite effect on the size of impedance arc (compare the insets of Fig. 6C and D). Therefore the combination of PAMT and sCPE can best facilitate the electron transfer kinetics for methanol oxidation among the four Pt supports.

Some interesting impedance patterns were observed in the middle potential range. At the potential of 0.5 V, the Nyquist plots of Pt/GCE and Pt/PAMT/sCPE showed an unusual and unapprehended inductive loop lying entirely in the first quadrant (Fig. 6A and D). More unexpectedly, the impedance pattern of Pt/GCE at 0.7 V displayed a reverse arc in the second quadrant that was different from the impedance arcs at potentials $\leq$0.65 V or $\geq$0.75 V (Fig. 6A). The reverse arc also occurred at Pt/PAMT/GCE even in a wider potential range, and the size of arc decreased with potential increasing from 0.5 to 0.7 V (Fig. 6B). The appearance of the reverse impedance pattern has been considered as a result of the change of rate determining step from CO_{ads} oxidation to CH_3OH oxidation as CO_{ads} [55]. This change occurred at Pt/PAMT/GCE in the wider potential range than at Pt/GCE, due to the GCE-supported PAMT film that increased the electron transfer resistance of CH_3OH oxidation as described above. The reversing of impedance arc to the second (and the third) quadrant(s) did not take place at both the sCPE-supported electrodes, which can be attributed to the faster

Table 3
Fitting parameters based on the equivalent circuit in Fig. 6E.

Electrode	E (V) vs. SCE	R_s (Ω cm^2)	Y_0(CPE$_1$) (mS s^n cm^{-2})	R_{ct1} (Ω cm^2)	Y_0(CPE$_2$) (mS s^n cm^{-2})	R_{ct2} (Ω cm^2)	R_L (Ω cm^2	L (H cm^2)
Pt/GCE	0.3	0.531	12.1 n = 1	108	1.36 n = 0.91	214	–	–
	0.4	0.523	3.96 n = 1	6.14	3.08 n = 0.83	105	0	1466
Pt/PAMT/GCE	0.3	0.628	4.26 n = 1	167	2.16 n = 0.89	133	–	–
	0.4	0.604	2.54 n = 0.76	31.8	1.72 n = 1	110	5.15	97.0
Pt/sCPE	0.3	0.672	12.9 n = 1	272	1.21 n = 0.86	367	–	–
	0.4	0.653	1.72 n = 0.83	38.1	3.03 n = 0.91	138	65.0	951
	0.5	0.667	2.52 n = 0.82	18.3	2.04 n = 0.96	385	78.9	298
Pt/PAMT/sCPE	0.3	0.940	16.1 n = 1	113	1.17 n = 0.92	270	–	–
	0.4	0.622	4.15 n = 0.81	12.9	2.57 n = 1	86.8	21.7	131

electron transfer kinetics of CH_3OH oxidation at them, especially at Pt/PAMT/sCPE.

3.6. Chronoamperometric studies

Chronoamperometry data were recorded at 0.81 V (vs. RHE) for 1200s as a measure of the catalyst deactivation for Pt/sCPE and Pt/PAMT/sCPE (Fig. 7). It has been reported that, at Pt bulk electrodes, the methanol oxidation currents in chronoamperograms decayed rapidly with time due to the CO induced poisoning and was almost zero after 500 s [26,56], whereas at the same time, the currents at Pt nanoparticles were still about one fifth [26] or one sixth [56] of the initial values. The results after continuous runs for 2000s were reported for the Pt nanowires supported on Pt gauze, pristine Pt gauze, E-TEK and W gauze, showing that the current densities decayed to about 8.4%, 9.4%, 9.5%, and 6.4%, respectively, of their initial values [57]. In the present work, the current densities shown in Fig. 7 decreased markedly at first, but then became relatively stable. After 1200s of continuous operation, the current densities at the Pt/sCPE and Pt/PAMT/sCPE were about 20% and 23% of the initial values, respectively, and the current at the latter was 2.5 times that at the former due to the role of PAMT. By comparison, the Pt particles supported on sCPE and on PAMT/sCPE exhibited a slower current decay over time. The higher tolerance to CO-like intermediates may be attributed to a faster removal rate of the poisoning species on the sharp nanothorns arranged on the particle surface.

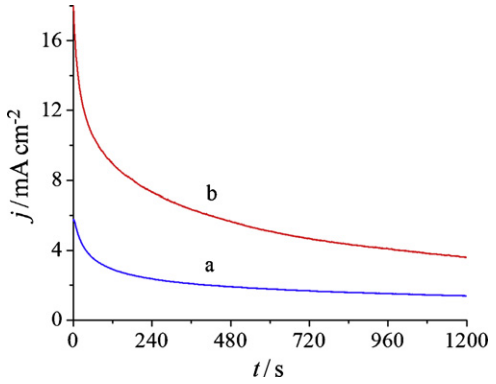

Fig. 7. Chronoamperograms for methanol oxidation in 0.5 mol dm^{-3} CH_3OH + 0.5 mol dm^{-3} H_2SO_4 at 0.81 V (vs. RHE) on Pt/sCPE (a) and Pt/PAMT/sCPEs (b). The electrodes were prepared under the same conditions as in Fig. 2.

4. Conclusions

Platinum particles are comparatively deposited on four carbon-based supports: GCE, sCPE, PAMT/GCE and PAMT/sCPE. The particles formed on all the supports show an impressive chestnut bur-like morphology with numerous nanothorns that is favorable for improving catalytic activity due to the highly developed specific surface. On the PAMT films supported on the both substrates, the deposited particles are found in two size fractions (<1 μm and 2–3 μm), which may provide high concentration of surface defects and therefore enhanced activity. Both the sCPE and the PAMT contribute to increase the electrochemical active area of Pt catalyst and therefore have a positive effect on catalytic activity, in comparison with the GCE and the uncoated supports, respectively. Moreover, the sCPE-supported PAMT facilitates the electron transfer kinetics of the oxidation of methanol, whereas the GCE-supported PAMT gives an opposite effect on the electron transfer. Based on above, the Pt/PAMT/sCPE generates the highest voltammetric current density upon methanol oxidation among the four Pt supports. These findings offer insight into the combination of solid carbon paste and a conducting polymer as a promising support of Pt catalyst in direct methanol fuel cell.

Acknowledgment

The authors gratefully acknowledge the financial support from the National Nature Science Foundation of China (No. 20972038).

References

[1] S.K. Kamarudin, A.M. Zainoodin, W.R.W. Daud, Int. J. Hydrogen Energy 35 (2010) 4606–4621.
[2] M. Zhiani, B. Rezaei, J. Jalili, Int. J. Hydrogen Energy 35 (2010) 9298–9305.
[3] P.G. Pickup, R.B. Moghaddam, Electrochem. Commun. 13 (2011) 704–706.
[4] E. Yoo, T. Okada, T. Kizuka, J. Nakamura, J. Power Sources 180 (2008) 221–226.
[5] V.M. Jovanović, S. Terzić, A.V. Tripković, K.D. Popović, J.D. Lović, Electrochem. Commun. 6 (2004) 1254–1258.
[6] C. Paoletti, A. Cemmi, L. Giorgi, R. Giorgi, L. Pilloni, E. Serra, M. Pasquali, J. Power Sources 183 (2008) 84–91.
[7] L. Dong, Q. Liu, L. Wang, K. Chen, in: S. Mikhailov (Ed.), Physics and Applications of Graphene—Experiments, InTech, 2011, pp. 525–540.
[8] S.J. Park, J.M. Park, M.K. Seo, J. Colloid Interface Sci. 337 (2009) 300–303.
[9] C.K. Rhee, B.J. Kim, C. Ham, Y.J. Kim, K. Song, K. Kwon, Langmuir 25 (2009) 7140–7147.
[10] K.-W. Park, Y.-E. Sung, J. Phys. Chem. B 108 (2004) 939–944.
[11] L. Calvillo, M. Gangeri, S. Perathoner, G. Centi, R. Moliner, M.J. Lázaro, Int. J. Hydrogen Energy 36 (2011) 9805–9814.
[12] W.Q. Zhou, Y.K. Du, F.F. Ren, C.Y. Wang, J.K. Xu, P. Yang, Int. J. Hydrogen Energy 35 (2010) 3270–3279.

[13] C.C. Yang, T.Y. Wu, H.R. Chen, T.H. Hsieh, K.S. Ho, C.W. Kuo, Int. J. Electrochem. Sci. 6 (2011) 1642–1654.
[14] T. Maiyalagan, B. Viswanathan, Mater. Chem. Phys. 121 (2010) 165–171.
[15] H. Razmi, E. Habibi, H. Heidari, Electrochim. Acta 53 (2008) 8178–8185.
[16] H. Razmi, E. Habibi, J. Solid State Electrochem. 13 (2009) 1897–1904.
[17] E. Antolini, Appl. Catal. B: Environ. 100 (2010) 413–426.
[18] Z.A. Hu, L.J. Ren, X.J. Feng, Y.P. Wang, Y.Y. Yang, J. Shi, L.P. Mo, Z.Q. Lei, Electrochem. Commun. 9 (2007) 97–102.
[19] M.F. Ahmed, K.L. Nagashree, N.H. Raviraj, Electrochim. Acta 55 (2010) 2629–2635.
[20] T. Maiyalagan, J. Power Sources 179 (2008) 443–450.
[21] N. Munichandraiah, S. Patra, S. Dash, V. Anand, C.S. Nimisha, G.M. Rao, Mater. Sci. Eng. B: Adv. 176 (2011) 785–791.
[22] N. Munichandraiah, S. Patra, Langmuir 25 (2009) 1732–1738.
[23] T. Spătaru, M. Marcu, L. Preda, P. Osiceanu, J.M.C. Moreno, N. Spătaru, J. Solid State Electrochem. 15 (2010) 1149–1157.
[24] Y.X. Li, Y.A. Zhou, H.Y. Xian, F. Li, S.N. Wu, Q.F. Lu, L. Wang, Electrochim. Acta 55 (2010) 5905–5910.
[25] A. Galal, N.F. Atta, S.A. Darwish, S.M. Ali, Top. Catal. 47 (2008) 73–83.
[26] B. Habibi, M.H. Pournaghi-Azar, J. Solid State Electrochem. 14 (2010) 599–613.
[27] C.M. Jiang, X.Q. Lin, J. Power Sources 164 (2007) 49–55.
[28] J.B. Raoof, R. Ojani, S.R. Hosseini, Int. J. Hydrogen Energy 36 (2011) 52–63.
[29] E. Antolini, E.R. Gonzalez, Appl. Catal. A: Gen. 365 (2009) 1–19.
[30] E.H.V. Broekhoven, J.W.F.M. Schoonhoven, V. Ponec, Surf. Sci. 156 (1985) 899–910.
[31] R. Ojani, J.B. Raoof, S. Fathi, S. Alami-Valikchali, J. Solid State Electrochem. 15 (2011) 1935–1941.
[32] R. Ojani, J.B. Raoof, S.R.H. Zavvarmahalleh, Electrochim. Acta 53 (2008) 2402–2407.
[33] J.B. Raoof, M.A. Karimi, S.R. Hosseini, S. Mangelizadeh, J. Electroanal. Chem. 638 (2010) 33–38.
[34] K.L. Nagashree, M.F. Ahmed, J. Solid State Electrochem. 14 (2010) 2307–2320.
[35] L. Zheng, J.F. Song, J. Solid State Electrochem. 14 (2010) 43–50.
[36] J.B. Raoof, R. Ojani, S.R. Hosseini, J. Power Sources 196 (2011) 1855–1863.
[37] R. Ojani, J.-B. Raoof, S. Fathi, J. Solid State Electrochem. 13 (2009) 927–934.
[38] I. S˘vancara, K. Vytr˘as, K. Kalcher, A. Walcarius, J. Wang, Electroanalysis 21 (2009) 7–28.
[39] I. Švancara, A. Walcarius, K. Kalcher, K. Vytřas, Cent. Eur. J. Chem. 7 (2009) 598–656.
[40] V. Rajendran, E. Csöregi, Y. Okamoto, L. Gorton, Anal. Chim. Acta 373 (1998) 241–251.
[41] J.-B. He, F. Qi, Y. Wang, N. Deng, Sens. Actuators B: Chem. 145 (2010) 480–487.
[42] J.J. Mallett, E.B. Svedberg, J.E. Bonevich, A.J. Shapiro, W.F. Egelhoff, T.P. Moffat, J. Electrochem. Soc. 155 (2008) D1–D9.
[43] F. Maillard, S. Schreier, M. Hanzlik, E.R. Savinova, S. Weinkauf, U. Stimming, Phys. Chem. Chem. Phys. 7 (2005) 385–393.
[44] X.J. Huang, O. Yarimaga, J.H. Kim, Y.K. Choi, J. Mater. Chem. 19 (2009) 478–483.
[45] A.J. Bard, L.R. Faulkner, Electrochemical Methods: Fundamentals and Applications, 2nd ed., John Wiley & Sons, New York, 2001, pp. 496–499.
[46] T. Iwasita, Electrochim. Acta 47 (2002) 3663–3674.
[47] Z.H. Wang, G.Q. Gao, H.F. Zhu, Z.D. Sun, H.P. Liu, X.L. Zhao, Int. J. Hydrogen Energy 34 (2009) 9334–9340.
[48] R. Ojani, J.B. Raoof, S. Fathi, Electrochim. Acta 54 (2009) 2190–2196.
[49] J.T. Müller, P.M. Urban, W.F. Hölderich, J. Power Sources 84 (1999) 157–160.
[50] D.A. Harrington, B.E. Conway, Electrochim. Acta 32 (1987) 1703–1712.
[51] S.H. Yang, C.Y. Chen, W.J. Wang, J. Power Sources 195 (2010) 2319–2330.
[52] M. Jafarian, I. Danaee, F. Forouzandeh, F. Gobal, M.G. Mahjani, Int. J. Hydrogen Energy 34 (2009) 859–869.
[53] W. Sugimoto, K. Aoyama, T. Kawaguchi, Y. Murakami, Y. Takasu, J. Electroanal. Chem. 576 (2005) 215–221.
[54] P. Kalimuthu, S.A. John, Electrochem. Commun. 11 (2009) 367–370.
[55] I.-M. Hsing, X. Wang, Y.-J. Leng, J. Electrochem. Soc. 149 (2002) A615–A621.
[56] Z.F. Chen, Y.X. Jiang, Y. Wang, J.M. Xu, L.Y. Jin, S.G. Sun, J. Solid State Electrochem. 9 (2005) 363–370.
[57] E.P. Lee, Z. Peng, W. Chen, S. Chen, H. Yang, Y. Xia, ACS Nano 2 (2008) 2167–2173.